Atmospheric Environment: X 1 (2019) 100006

Contents lists available at ScienceDirect

Atmospheric Environment: X

journal homepage: www.journals.elsevier.com/atmospheric-environment-x

A note on flow behavior in axially-dispersed plug flow reactors with step input of tracer☆

Yuanlong Huang[a], John H. Seinfeld[b,*]

[a] Division of Geological and Planetary Science, California Institute of Technology, Pasadena, CA, 91125, USA
[b] Division of Chemistry and Chemical Engineering, California Institute of Technology, Pasadena, CA, 91125, USA

HIGHLIGHTS

- Cumulative RTD can be used to characterize flow conditions in flow reactors.
- Step injection is recommended to measure cumulative RTD.
- Derivation of the analytical expression of cumulative RTD in AD-PFR model.

ARTICLE INFO

Keywords:
Plug flow reactor
Axial dispersion
Step injection
Residence time distribution

ABSTRACT

Atmospheric chemistry studies are frequently conducted in flow reactors, such as the potential aerosol mass (PAM) reactor. To characterize the flow condition in such a reactor, an axially-dispersed plug flow reactor (AD-PFR) model has been applied to explain the observed residence time distribution (RTD). Compared with the traditional RTD analysis that directly fits the observed data from a pulse input or differentiates the data points from a step input, we introduce here a direct method to retrieve the axial diffusivity in an AD-PFR model by fitting an analytical formula to the rising profile of the tracer at the beginning of the experiment (the transition data before the reactor reaches steady state). This method can be readily used to determine the flow conditions inside an AD-PFR.

1. Introduction

Flow reactors have achieved a prominent status in the study of atmospheric chemistry. The nature of the flow in such reactors plays a role in interpretation of the kinetic data obtained within the reactor. For a cylindrical flow reactor with sufficiently low Reynolds number (Re), the fluid velocity field is parabolic laminar flow. After a sufficient distance downstream, a radial velocity gradient-induced concentration difference can be smoothed by radial molecular diffusion. In this case, the three-dimensional tubular transport becomes essentially a one-dimensional convective-diffusive flow known as Taylor dispersion (Taylor, 1953). Temperature differences between the fluid and the reactor wall may also serve to perturb the ideal parabolic profile and induce radial mixing (Huang et al., 2017). An axially-dispersed plug flow reactor (AD-PFR) model applies in these situations of non-ideal, low-Re flow reactors.

To better understand the chemical kinetics in the flow tube reactor within the AD-PFR framework, the two necessary parameters are the intensity of axial dispersion and the average residence time, which can be derived from the residence time distribution (RTD) of a tracer that is non-interactive with the wall. Then the AD-PFR model can be parameterized to reproduce experimental data. In addition to simulation, the parameters can be used to adjust the measured oxidation exposure (residence time × concentration, e.g., OH exposure, Huang et al., 2017), a common quantity to represent the degree of oxidation occurring in an oxidation flow reactor. In all cases, the RTD plays an important role in evaluating these parameters.

The residence time distribution (RTD), often referred to as an *E*-curve, is widely used to diagnose the physics of the transport in such flow reactors. An *E*-curve is generated by a pulse or step injection, with the temporal concentration profile being monitored at the outlet of the reactor. Measurement of the RTD at the exit of the reactor affords an analysis of the chemical kinetics occurring in the reactor (Li et al., 2015; Peng et al., 2015). A pulse input of tracer requires injection of a quantity of tracer within a period of time much shorter than the average residence time in the reactor; on the other hand, a step input requires a

☆ This is a Technical Note.

* Corresponding author.
E-mail address: seinfeld@caltech.edu (J.H. Seinfeld).

https://doi.org/10.1016/j.aeaoa.2019.100006
Received 1 October 2018; Received in revised form 3 January 2019; Accepted 5 January 2019
Available online 24 January 2019

stable and constant source of tracer. The step input affords a smoother *E*-curve from which the rising portion of the curve (known as the *F*-curve) can be obtained more easily. Mitroo et al. (2018) also reported the step-down method, in which a reactor initially filled with tracer is replaced by clean air, and from which an *E*-curve with a smooth tail can be obtained. In summary, analysis of experimental data on the nature of flow in the flow reactor generally includes: (1) direct *E*-curve fitting from a pulse input (Lambe et al., 2011; Huang et al., 2017; Simonen et al., 2017); (2) *E*-curve fitting by differentiating the *F*-curve from a step input of tracer (Mitroo et al., 2018); (3) *F*-curve fitting from the cumulative *E*-curve with a pulse input (Wolf and White, 1976).

We suggest here a fourth method to diagnose the nature of flow in a flow reactor, that is, analyzing the *F*-curve from a step input by directly fitting the observed concentration distribution to the analytical solution of the AD-PFR model with a continuous source of tracer. In this approach, differentiation of the *F*-curve is not required. This method takes advantage of the time-dependent data prior to the reactor reaching steady state. Such an approach can be carried out at the inception of an experiment. Two critical parameters relating to the behavior the flow reactor, i.e., the axial diffusivity $\mathscr{D}$ and the average residence time in the reactor, τ_r, can be obtained from fitting a reactor model to the *F*-curve. Since the volumetric flow rate through the reactor and the diameter of the reactor are known, τ_r can be replaced with the effective length L of the reactor. By comparison with those parameters derived from injection of a pulse of tracer, we show that the direct fitting of data from a step input to the *F*-curve has the potential to be applied in the same situations as those to the *E*-curve. Since the flow condition for the measurement of the *F*-curve is the same as that in an actual experiment, i.e., continuous rather than pulse injection, parameters derived from the *F*-curve may be better representative of the AD-PFR model.

2. Formulation and solution

The conservation equation describing the AD-PFR is:

$$\frac{\partial c(x,\,t)}{\partial t} = -u\frac{\partial c(x,\,t)}{\partial x} + \mathscr{D}\frac{\partial^2 c(x,\,t)}{\partial x^2} \tag{1}$$

where c is the concentration of the tracer, x and t are the variables of axial distance and time, u is the uniform convective velocity, and $\mathscr{D}$ is the axial diffusivity.

For a pulse input, the dimensionless RTD (*E*-curve) is

$$E_{\text{pulse}}(\theta) = \sqrt{\frac{\text{Pe}}{4\pi\theta}}\exp\left[-\frac{(1-\theta)^2}{4\theta/\text{Pe}}\right] \tag{2}$$

where $\text{Pe} = \frac{Lu}{\mathscr{D}}$ is the Péclet number, L is the length of the reactor, $\theta = \frac{t}{\tau_r}$, and $\tau_r = \frac{L}{u}$ is the average residence time in the reactor.

In reality, the pulse input usually persists for a short period of time (square-wave injection), e.g., τ_0, which should be $\ll \tau_r$. The *E*-curve can be described as (Huang et al., 2017):

$$E_{\text{period}}(\theta) = \frac{1}{2}\left[\text{erf}\left(\frac{1-\theta}{\sqrt{4\theta/\text{Pe}}}\right) - \text{erf}\left(\frac{1-\theta-\theta_0}{\sqrt{4\theta/\text{Pe}}}\right)\right] \tag{3}$$

where $\theta_0 = \frac{\tau_0}{\tau_r}$ and $\text{erf}(x) = \frac{2}{\sqrt{\pi}}\int_0^x \exp(-\eta^2)d\eta$.

With a fixed source at $x = 0$, i.e., $c(0,\,t) = c_0$, into an initially empty reactor, i.e., $c(x,\,0) = 0$, the downstream concentration far from the source remains 0, i.e., $c(+\infty,\,t) = 0$, for which an analytical solution exists (Ogata and Banks, 1961), the derivation of which is given in Appendix A. The dimensionless form of the temporal profile of the tracer at the end of the AD-PFR for the step input (*F*-curve) is

$$F_{\text{step}}(\theta) = \frac{1}{2}\left[\text{erfc}\left(\frac{1-\theta}{\sqrt{4\theta/\text{Pe}}}\right) + \exp(\text{Pe})\text{erfc}\left(\frac{1+\theta}{\sqrt{4\theta/\text{Pe}}}\right)\right] \tag{4}$$

where $\text{erfc}(x) = 1 - \text{erf}(x)$. Note that even though by definition the *F*-curve is the cumulative distribution function of the *E*-curve, Eq. (4) is not the integral form of Eq. (2), since to derive Eq. (2) only needs an initial condition but two more boundary conditions are necessary to obtain Eq. (4).

Another common treatment of the AD-PFR model applies the so-called Danckwerts boundary conditions (Danckwerts, 1953). Instead of a fixed source at $x = 0$, a constant flux is assumed: upstream of $x = 0$ only convection holds, while downstream of $x = 0$ both convection and dispersion occur, leading to

$$uc(0_-,\,t) = uc(0_+,\,t) - \mathscr{D}\frac{\partial c(0_+,\,t)}{\partial x} \tag{5}$$

where $c(0_-,\,t)$ and $c(0_+,\,t)$ are concentrations right before and after the entrance ($x = 0$) of the reactor. Eq. (5) indicates that the concentration profile at $x = 0$ is non-continuous, and as axial dispersion increases, the difference between $c(0_-,\,t)$ and $c(0_+,\,t)$ gets larger. Correspondingly, Danckwerts (1953) suggested a smooth profile of the concentration at $x = L$, i.e.,

$$\frac{\partial c(L,\,t)}{\partial x} = 0 \tag{6}$$

A closed-form analytical solution to this case does not exist, but a numerical solution can be applied (see Appendix B). To be consistent with Eq. (4), the reactor is assumed to be initially empty, i.e., $c(x,\,0) = 0$.

To distinguish between the cases of Eq. (4) and the numerical solution of Eqs. (5) and (6), we refer to them as AD-PFR and Danckwerts, respectively. Compared with the continuity of tracer flux at the inlet as specified by Eq. (5), the inlet boundary condition in the AD-PFR requires a step change in diffusivity at the inlet of the reactor.

Fig. 1 shows the calculated solutions of the *F*-curves for PFR, continuous stirred-tank reactor (CSTR), tubular laminar flow reactor (LFR), AD-PFR, and Danckwerts models. With the same extent of axial dispersion (Pe = 10, the same order of magnitude as those of typical flow tube reactors), the tracers in the AD-PFR and the Danckwerts models behave similarly, suggesting that the effects of different boundary conditions on the temporal profiles are limited under typical flow tube reactor operation conditions and both models can represent actual condition.

3. Experimental

Experiments were performed in the Caltech Photochemical Oxidation flow Tube reactor (CPOT, Huang et al., 2017). Briefly, the

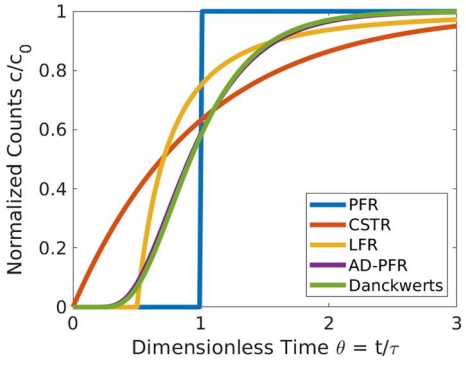

Fig. 1. Theoretical temporal profiles (*F*-curve) of the tracer emerging from a flow reactor as described in different models. The analytical dimensionless expression for PFR is $F_{\text{PFR}}(\theta) = H(\theta - 1)$, for CSTR is $F_{\text{CSTR}}(\theta) = 1 - \exp(-\theta)$, for tubular LFR is $F_{\text{LFR}}(\theta) = H\left(\theta - \frac{1}{2}\right)\left(1 - \frac{1}{(2\theta)^2}\right)$, for AD-PFR is Eq. (4) (Pe = 10), and for Danckwerts AD-PFR is numerical simulation (Pe = 10), where $H(x-a)$ is the Heaviside step function, i.e., $H(x-a) = 0$ as $x < a$, $H(x-a) = 0.5$ as $x = a$, and $H(x-a) = 1$ as $x > a$. Note that *F*-curves for AD-PFR and Danckwerts AD-PFR are similar when axial dispersion (Pe) is the same.

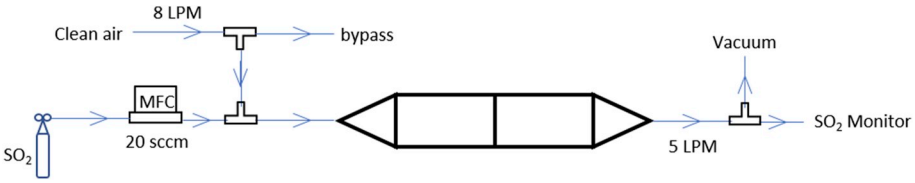

Fig. 2. Experimental setup.

CPOT comprises a conic transition tube (53 cm) as the inlet, two straight quartz tubes (1.2 m × 17 cm I.D. each) as the main reactor, and a second conic tube (53 cm) to produce a cup-mixed-average output. A SO^2 cylinder of 10 ppm (Airgas) served as the source of tracer, and a SO^2 monitor (model 43i, ThermoFisher) was applied to record the temporal profile of SO^2 at the outlet (Fig. 2). The overall volumetric flow rate through the CPOT was fixed at 5 L min^{-1} (Re ~ 20) at room temperature (~ 297 K). Prior to injection, purified clean air flowed through the reactor. Both pulse and step injections of SO^2 were carried out. The pulse injection lasted for 1 min with the flow of SO^2 set at 100 sccm. For the step injection, the start of the experiment was recorded at the inception of SO^2 flow at 100 sccm by a mass flow controller. For each type of injection, the experiment was repeated for at least three times. Since the flow system at the inlet is open to the ambient, the additional injection of SO^2 is supposed not to perturb the flow field inside the reactor. The experiments were carried out under dry condition (RH < 1%), since SO^2 can interact strongly with the wall at high RH (Lambe et al., 2011) while Eq. (1) (and its solutions) does not incorporate this effect.

Fig. 3 shows typical temporal patterns of tracer corresponding to the pulse (green circles) and step (blue circles) injections, respectively. Data points represent 1 s resolution.

4. Results and discussion

The average residence time in the flow tube itself is ~ 510 s. Accounting for the two conic sections of the overall reactor assembly, the expected average residence time in the entire reactor assembly should exceed 510 s. With a pulse input lasting a period of 60 s, Eq. (3) is used to fit the observed data by the function fit in MATLAB (2016b). The parameter values obtained from the fitting are: $\mathscr{D}_{eq3} = (7.1 \pm 0.1) \times 10^{-4}$ m^2 s^{-1}, $\tau_{eq3} = 588 \pm 1$ s, and $L_{eq3} = 2.77 \pm 0.01$ m, with a $Pe_{eq3} = 18$. The inferred value of $\mathscr{D}_{eq3}$ is at least one order of magnitude larger than the inherent gas-phase molecular diffusivity of SO^2, confirming that the derived value of the diffusivity is a result of the fluid field. This eddy-like diffusivity is consistent with the observation in Huang et al. (2017). The fitted effective length of the reactor exceeds that solely of the reactor section (2.4 m), reflecting the role of the two conic sections at the inlet and outlet.

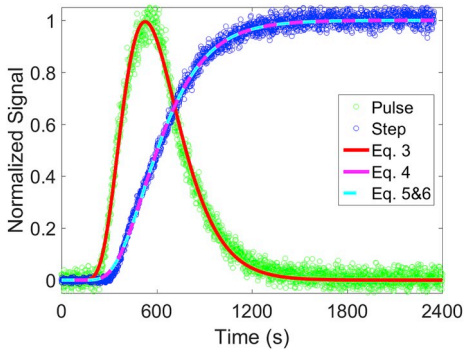

Fig. 3. Experimental profiles with pulse injection (green circles) fitted by Eq. (3) (red solid line) and step input (blue circles) fitted by AD-PFR model (Eq. (4), magenta solid line) as well as the Danckwerts boundary condition model (Eq. (5)&(6), cyan dashed line).

Experimental data from the step input suggest that none of the PFR, CSTR, or LFR models explains the observation, whereas both the AD-PFR and Danckwerts models show strong potential to fit the data. Fitting results by both models are shown together with observations in Fig. 3. Both models fit the data with $R^2 > 0.99$, further demonstrating the 1D-convective-diffusive plug flow reactor model as a representation of the CPOT reactor. The fitting results from Eq. (4) are: $\mathscr{D}_{eq4} = (1.09 \pm 0.02) \times 10^{-3}$ m^2 s^{-1}, $\tau_{eq4} = 648 \pm 2$ s, and $L_{eq4} = 3.05 \pm 0.02$ m, with $Pe_{eq4} = 13$. Those from Eqs. (5) and (6) are: $\mathscr{D}_{eq5} = (1.18 \pm 0.02) \times 10^{-3}$ m^2 s^{-1}, $\tau_{eq5} = 651 \pm 2$ s, and $L_{eq5} = 3.07 \pm 0.02$ m, with $Pe_{eq5} = 12$.

Eqs. (5) and (6) predictions of $\mathscr{D}$, τ, and L are close to those of Eq. (4), consistent with the theoretical prediction (Fig. 1). As a result, the inferred values of the Péclet number, Pe, are similar, suggesting that, in the present case, either model can be used to characterize the reactor. Fig. 3 also shows that the predictions of Eqs. (4) and (5)-(6) overlap closely. The comparison above suggests that Eq. (4) can be used as an inverse model to derive key parameters, e.g., $\mathscr{D}$, τ, and L, from the transitional profiles, because it has an analytical expression; while Danckwerts conditions are more practicable computationally, especially for the purpose of simulating nonlinear reactions and calculating OH exposure. Note that when modeling photochemical processes, the radiation intensity in the conical section can be much weaker than that in the main reactor; thus the length of the main reactor (as well as the residence time in the reaction section) should be used in the model instead of the effective length L (or τ) fitted from the E- or F-curves, while the diffusivity $\mathscr{D}$ stay the same.

The observed F-curve with step input started to rise ~ 35 s later than the observed E-curve with pulse input, consistent with the fitted average residence time that $\tau_F > \tau_E$. Moreover, the axial diffusivities derived from the F-curve exceed that derived from the E-curve. The Pe number inferred from F-curve is ~ 30 % smaller than that inferred from E-curve, indicating that though the pulse and step injection methods are similar the axial dispersion is larger in the step injection. This conclusion suggests that the fluid field may be slightly different in the two cases. Since the working conditions of the flow tube for the measurement of the F-curve are similar to those of actual flow tube experiments, i.e., precursors are injected continuously rather than in pulses, the larger extent of axial dispersion by fitting of the F-curve may better reflect the actual conditions inside the reactor.

We attempted to differentiate the F-curve from both step-up and step-down injection to obtain the E-curve, following Mitroo et al. (2018), which, however, given the relatively finer data point resolution, the potential lack of smoothness in the E-curve precludes as close fitting as with the pulse injection method. Lambe et al. (2011) show that inside the Potential Aerosol Mass (PAM) reactor two fluid field patterns exist, and thus the measured RTD is a superposition of two axially dispersed plug flows. The concept of superposition of two different flow patterns also applies to Eq. (4) since the number of unknown parameters is the same. Note that the idea of fitting the F-curve directly also applies for other theoretical residence time models, such as tanks-in-series (Mitroo et al., 2018), the advantages of which are: (1) the theories behind the F-curve are the same as those of the E-curve; (2) the experimental conditions needed to obtain the F-curve are similar to those actually performed, and (3) fewer data fluctuations exist relative to E-curve, since F-curve is always rising until it reaches steady state.

5. Conclusions

The axially-dispersed plug flow reactor (AD-PFR) model has shown potential to represent non-ideal reactors, the evidence for which is excellent fitting of the experimental data. We present here the successful application of fitting experimental data to the theoretical cumulative curve (the *F*-curve), which is a close representation of an actual tracer experiment. The derived parameters from the *F*-curve suggest relatively stronger axial dispersion than that suggested by the *E*-curve, which better represents the actual experimental condition in flow tube reactors, i.e., continuous injection of precursors rather than pulse injections.

We note here that though AD-PFR can be used to describe the residence time in non-ideal flow reactors, this model does not consider the interaction between the wall and the flow which is a common phenomenon, especially in sampling tubes (Pagonis et al., 2017). A gas-wall partition and convection model has been proposed to explain the observed signal delay that can occur from a step injection, which is beyond the treatment of this technical note.

Acknowledgement

YH acknowledges helpful discussions with I-Te Lu.

Supplementary data

Supplementary data to this article can be found online at https://doi.org/10.1016/j.aeaoa.2019.100006.

Appendix A. Derivation of PDE solution

The partial differential equation (PDE) describing an axially-dispersed plug flow reactor (AD-PFR) is

$$\frac{\partial c(x,t)}{\partial t} = -u\frac{\partial c(x,t)}{\partial x} + \mathscr{D}\frac{\partial^2 c(x,t)}{\partial x^2} \tag{A.1}$$

When there is a fixed source at $x = 0$, Eq. (A.1) is subject to the following initial and boundary conditions (Eqs. (A.2)-(A.4)):

$$c(x,0) = 0 \tag{A.2}$$

$$c(0,t) = c_0 \tag{A.3}$$

$$c(+\infty,t) = 0 \tag{A.4}$$

Separation of variables or similarity solutions are not available here. Since the range of x is 0 to infinity, the method of Fourier transform does not apply. Ogata and Banks (1961) proposed the transformation

$$c(x,t) = \Gamma(x,t)\exp\left(\frac{ux}{2\mathscr{D}} - \frac{u^2 t}{4\mathscr{D}}\right) \tag{A.5}$$

and applied Duhamel's theorem to derive the solution; thus the solution (Eq. (4)) of Eqs. (A.1)-(A.4) is referred to as the Ogata-Banks Formula. The introduction of Eq. (A.5) transforms Eq. (A.1) into a pure diffusion equation but the boundary condition Eq. (A.3) becomes t-dependent, making the solution more complicated. The derivation we introduce here involves basic knowledge of complex analysis, in order to solve Eqs. (A.1)-(A.4).

First, we use the method of Laplace transform with respect to t, i.e.,

$$c(x,t) \to \mathscr{L}\{c(x,t)\}(x,s) = \int_0^\infty c(x,t)\exp(-st)dt = L(x,s) \tag{A.6}$$

To do this, multiplying both sides of Eq. (A.1) by $\exp(-st)$, and integrating from 0 to $+\infty$ with respect to t, the first term of Eq. (A.1) becomes $sL(x,s) - c(x,0)$ after integration by parts. The other two terms keep the same form because of linearity of the operator. Rearranging the equation, Eq. (A.1) becomes:

$$sL(x,s) - c(x,0) + u\frac{\partial L(x,s)}{\partial x} = \mathscr{D}\frac{\partial^2 L(x,s)}{\partial x^2} \tag{A.7}$$

which can be rearranged as:

$$\mathscr{D}\frac{\partial^2 L}{\partial x^2} - u\frac{\partial L}{\partial x} - sL = 0 \tag{A.8}$$

And boundary condition Eqs. (A.3) and (A.4) become:

$$\mathscr{L}\{C(0,t)\} = L(0,s) = \frac{c_0}{s} \tag{A.9}$$

$$\mathscr{L}\{C(\infty,t)\} = L(\infty,s) = 0 \tag{A.10}$$

The general solution for Eq. (A.8) is

$$L(x,s) = A\exp(\lambda_1 x) + B\exp(\lambda_2 x) \tag{A.11}$$

where $\lambda_1 = \frac{u+\sqrt{u^2+4\mathscr{D}s}}{2\mathscr{D}}$ and $\lambda_2 = \frac{u-\sqrt{u^2+4\mathscr{D}s}}{2\mathscr{D}}$. With Eqs. (A.9) and (A.10) we get $A = 0$ and $B = \frac{c_0}{s}$. So the solution for Eq. (A.8) is

$$\begin{aligned} L(x,s) &= \frac{c_0}{s}\exp\left(\frac{u-\sqrt{u^2+4\mathscr{D}s}}{2\mathscr{D}}x\right) \\ &= c_0\exp\left(\frac{ux}{2\mathscr{D}}\right)\frac{1}{s}\exp\left(-\frac{x}{\sqrt{\mathscr{D}}}\sqrt{\frac{u^2}{4\mathscr{D}}+s}\right) \end{aligned} \tag{A.12}$$

Then the key problem is how to obtain the inverse Laplace transform (iLT) to Eq. (A.12). We can simplify it in the form of $\frac{A}{s}\exp(-B\sqrt{C+s})$, where $A = c_0\exp\left(\frac{ux}{2\mathscr{D}}\right)$, $B = \frac{x}{\sqrt{\mathscr{D}}}$, $C = \frac{u^2}{4\mathscr{D}}$. After applying the Bromwich contour integral over the complex plane (Fig. A1), we will get the iLT result. We note here that the iLT result (Eq. (A.22)) can be verified by Mathematica (Wolfram), a detailed step-by-step contour integration of iLT is provided here.

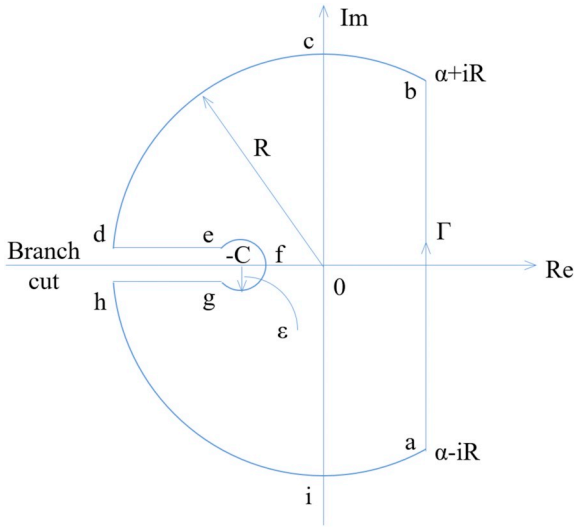

Fig. A.1. Bromwich integral path over complex plane.

The iLT is in the form of

$$f(t) = \mathscr{L}^{-1}\{L(s)\} = \frac{1}{2\pi i}\int_{\alpha-i\infty}^{\alpha+i\infty} L(s)\exp(st)ds$$
$$= \frac{1}{2\pi i}\int_{\alpha-i\infty}^{\alpha+i\infty} \frac{A}{s}\exp(-B\sqrt{C+s} + st)ds \tag{A.13}$$

The integral of Eq. (A.13) is on a complex plane along a vertical line $s = \alpha$ from $-i\infty$ to $+i\infty$, where α can be any value right of all singularities (poles, branch points, etc.). The Method of Residues will be applied to evaluate this integral, which states that the integration along a closed curve on a complex plane equals the sum of residues at all isolated singularities. Thus we construct a counterclockwise loop Γ as shown in Fig. A1, also known as the Bromwich contour, to evaluate the integral. Note that there is a branch point at $s = -C$ (thus a branch cut from $-C$ to $-\infty$ in this case) and an isolated singular point at $s = 0$ on this contour. As $R \to \infty$, the path $\hat{ab}$ approaches that we are looking for. As $\lim_{R\to\infty}|L(s)| = 0$, by Jordan's Lemma, the integration over $\hat{bcd}$ and $\hat{hia}$ will be zero when $R \to \infty$. Since the integration over path $\hat{de}$, $\hat{efg}$, and $\hat{gh}$ can be calculated and the integration over the whole contour can be obtained by residue theorem, i.e.,

$$\oint_\Gamma = \lim_{R\to\infty}\left(\int_{\hat{ab}} + \int_{\hat{de}} + \int_{\hat{efg}} + \int_{\hat{gh}}\right) = \mathrm{Res}(0) \tag{A.14}$$

Then we can get $\lim_{R\to\infty}\int_{\hat{ab}} = \mathrm{Res}(0) - \lim_{R\to\infty}\left(\int_{\hat{de}} + \int_{\hat{efg}} + \int_{\hat{gh}}\right)$.

The residue at $s = 0$ is

$$\mathrm{Res}(0) = 2\pi i(A\exp(-B\sqrt{C+s} + st))|_{s=0} = 2\pi i\, A\exp(-B\sqrt{C}) \tag{A.15}$$

Over $\hat{de}$, we set $C + s = r\exp(i\pi) = -r$, then $\sqrt{C+s} = \sqrt{r}\exp\left(\frac{i\pi}{2}\right) = i\sqrt{r}$. So we get $ds = -dr$ and $\lim_{\varepsilon\to 0}\int_{-R}^{-C-\varepsilon} L(s)ds = -\lim_{\varepsilon\to 0}\int_{R-C}^{\varepsilon} L(r)dr = -\int_{R-C}^{0} L(r)dr$. The integration over $\hat{de}$ becomes:

$$\int_{\hat{de}} = -\int_{R-C}^{0}\frac{A}{-r-C}\exp(-iB\sqrt{r} + (-r-C)t)dr$$
$$= \int_{R-C}^{0}\exp(-(r+C)t)\frac{A}{r+C}\exp(-iB\sqrt{r})dr \tag{A.16}$$

Over $\hat{gh}$, we set $C + s = r\exp(-i\pi) = -r$, then $\sqrt{C+s} = \sqrt{r}\exp\left(-\frac{i\pi}{2}\right) = -i\sqrt{r}$ and also $ds = -dr$, and $\lim_{\varepsilon\to 0}\int_{-C-\varepsilon}^{-R} L(s)ds = -\lim_{\varepsilon\to 0}\int_{\varepsilon}^{R-C} L(r)dr = -\int_{0}^{R-C} L(r)dr$. The integration over $\hat{gh}$ becomes:

$$\int_{\hat{gh}} = -\int_{0}^{R-C}\frac{A}{-r-C}\exp(iB\sqrt{r} + (-r-C)t)dr$$
$$= \int_{0}^{R-C}\exp(-(r+C)t)\frac{A}{r+C}\exp(iB\sqrt{r})dr \tag{A.17}$$

Over $\hat{efg}$, we set $C + s = \varepsilon\exp(-i\theta)$, then $\sqrt{C+s} = \sqrt{\varepsilon}\exp\left(-\frac{i\theta}{2}\right)$. So we get $ds = -i\varepsilon\exp(i\theta)d\theta$ and

$$\lim_{\varepsilon\to 0}\int_{\hat{efg}} L(s)ds = \lim_{\varepsilon\to 0}\int_{\pi}^{-\pi} -\frac{A}{\varepsilon\exp(-i\theta)-C} i\varepsilon\exp(i\theta)$$
$$\exp\left[-B\sqrt{\varepsilon}\exp\left(-\frac{i\theta}{2}\right)+(\varepsilon\exp(-i\theta)-C)t\right]d\theta = 0 \tag{A.18}$$

Then we get:

$$\int_{\alpha-i\infty}^{\alpha+i\infty}\frac{A}{s}\exp(-B\sqrt{C+s}+st) = \lim_{R\to\infty}\int_{\hat{ab}} = \mathrm{Res}(0) - \lim_{R\to\infty}\left(\int_{\hat{de}}+\int_{\hat{efg}}+\int_{\hat{gh}}\right)$$
$$= 2\pi iA\exp(-B\sqrt{C}) - \lim_{R\to\infty}\int_{R-C}^{0}\exp(-(r+C)t)\frac{A}{r+C}\exp(-iB\sqrt{r})dr$$
$$-\lim_{R\to\infty}\int_{0}^{R-C}\exp(-(r+C)t)\frac{A}{r+C}\exp(iB\sqrt{r})dr$$
$$= 2\pi iA\exp(-B\sqrt{C}) - \int_{0}^{\infty}\frac{A\exp(-(r+C)t)}{r+C}(-\exp(-iB\sqrt{r})+\exp(iB\sqrt{r}))dr$$
$$= 2\pi iA\exp(-B\sqrt{C}) - 2iA\int_{0}^{\infty}\frac{\exp(-(r+C)t)}{r+C}\sin(B\sqrt{r})dr \tag{A.19}$$

Substituting Eq. (A.19) into Eq. (A.13) we get

$$f(t) = A\exp(-B\sqrt{C}) - A\int_{0}^{\infty}\frac{\exp(-(r+C)t)}{\pi(r+C)}\sin(B\sqrt{r})dr \tag{A.20}$$

It can be shown that (http://mathworld.wolfram.com/Erf.html):

$$\int_{0}^{\infty}\frac{\exp(-(x+p)t)}{\pi(x+p)}\sin(a\sqrt{x})dx =$$
$$-\sinh(a\sqrt{p}) + \frac{\exp(-a\sqrt{p})}{2}\mathrm{erf}\left(\frac{a}{2\sqrt{t}}-\sqrt{pt}\right) + \frac{\exp(a\sqrt{p})}{2}\mathrm{erf}\left(\frac{a}{2\sqrt{t}}+\sqrt{pt}\right) \tag{A.21}$$

where $\mathrm{erf}(x) = \frac{2}{\sqrt{\pi}}\int_0^x \exp(-\eta^2)d\eta$. So Eq. (A.20) becomes:

$$f(t) = \frac{A}{2}\exp(-B\sqrt{C})\mathrm{erfc}\left(\frac{B}{2\sqrt{t}}-\sqrt{Ct}\right) + \frac{A}{2}\exp(B\sqrt{C})\mathrm{erfc}\left(\frac{B}{2\sqrt{t}}+\sqrt{Ct}\right) \tag{A.22}$$

where $\mathrm{erfc}(x) = 1-\mathrm{erf}(x)$. Substituting A, B, and C into the above equation, the final iLT result of Eq. (A.13) is

$$c(x,t) = \frac{c_0}{2}\left[\mathrm{erfc}\left(\frac{x-ut}{\sqrt{4\mathscr{D}t}}\right) + \exp\left(\frac{xu}{\mathscr{D}}\right)\mathrm{eftc}\left(\frac{x+ut}{\sqrt{4\mathscr{D}t}}\right)\right] \tag{A.23}$$

Appendix B. Numerical solution of the Danckwerts boundary problem

We use the pde solver pdepe in MATLAB (2016b) to numerically solve the Danckwerts boundary problem. The code is available in the Supplementary Information.

References

Danckwerts, P.V., 1953. Continuous flow systems: distribution of residence times. Chem. Eng. Sci. 2 (1), 1–13.

Huang, Y., Coggon, M.M., Zhao, R., Lignell, H., Bauer, M.U., Flagan, R.C., Seinfeld, J.H., 2017. The Caltech Photooxidation Flow Tube reactor: design, fluid dynamics and characterization. Atmos. Meas. Tech. 10 (3), 839–867.

Lambe, A.T., Ahern, A.T., Williams, L.R., Slowik, J.G., Wong, J.P.S., Abbatt, J.P.D., Brune, W.H., Ng, N.L., Wright, J.P., Croasdale, D.R., Worsnop, D., Davidovits, P., Onasch, T.B., 2011. Characterization of aerosol photooxidation flow reactors: heterogeneous oxidation, secondary organic aerosol formation and cloud condensation nuclei activity measurements. Atmos. Meas.Tech. 4 (3), 445–461.

Li, R., Palm, B.B., Ortega, A.M., Hlywiak, J., Hu, W., Peng, Z., Day, D.A., Knote, C., Brune, W.H., de Gouw, J.A., Jimenez, J.L., 2015. Modeling the radical chemistry in an oxidation flow reactor: radical formation and recycling, sensitivities, and the oh exposure estimation equation. J. Phys. Chem. A 119 (19), 4418–4432.

Mitroo, D., Sun, Y., Combest, D.P., Kumar, P., Williams, B.J., 2018. Assessing the degree of plug flow in oxidation flow reactors (OFRs): a study on a potential aerosol mass (PAM) reactor. Atmos. Meas. Tech. 11 (3), 1741–1756.

Ogata, A., Banks, R., 1961. A solution of the differential equation of longitudinal dispersion in porous media. U. S. Geol. Surv. Prof. Pap. 34 411–A. URL. https://pubs.er.usgs.gov/publication/pp411A.

Pagonis, D., Krechmer, J.E., de Gouw, J., Jimenez, J.L., Ziemann, P.J., 2017. Effects of gas-wall partitioning in Teflon tubing and instrumentation on time-resolved measurements of gas-phase organic compounds. Atmos. Meas. Tech. 10 (12), 4687–4696.

Peng, Z., Day, D.A., Stark, H., Li, R., Lee-Taylor, J., Palm, B.B., Brune, W.H., Jimenez, J.L., 2015. HOx radical chemistry in oxidation flow reactors with low-pressure mercury lamps systematically examined by modeling. Atmos. Meas. Tech. 8 (11), 4863–4890.

Simonen, P., Saukko, E., Karjalainen, P., Timonen, H., Bloss, M., Aakko-Saksa, P., Rnkk, T., Keskinen, J., Dal Maso, M., 2017. A new oxidation flow reactor for measuring secondary aerosol formation of rapidly changing emission sources. Atmos. Meas. Tech. 10 (4), 1519–1537.

Taylor, G.I., 1953. Dispersion of soluble matter in solvent flowing slowly through a tube. Proc. Roy. Soc. Lond. A 219 (1137), 186–203.

Wolf, D., White, D.H., 1976. Experimental study of the residence time distribution in plasticating screw extruders. AIChE J. 22 (1), 122–131.